PNAS
www.pnas.org

Supplementary Information for

A complete biomechanical model of *Hydra* contractile behaviors, from neuron to muscle to movement

Hengji Wang, Joshua Swore, Shashank Sharma, John R Szymanski, Rafael Yuste, Thomas L Daniel, Michael Regnier, Martha M Bosma, Adrienne L Fairhall

Adrienne L Fairhall.
E-mail: fairhall@uw.edu

This PDF file includes:

Supplementary text
Figs. S1 to S11 (not allowed for Brief Reports)
Tables S1 to S5 (not allowed for Brief Reports)
Legends for Movies S1 to S2
SI References

Other supplementary materials for this manuscript include the following:

Movies S1 to S2

Supporting Information Text

Single cell model details

Here we give the details of the single cell model (Eq. 1 of the main text), and annotate their sources. Differential equations are solved using the Euler method with a step size of 0.2 ms.

Expressions. Ca^{2+} flux through IPR (1):

$$J_{\mathrm{IPR}} = k_{\mathrm{IPR}} \frac{C^2 P^2 R}{(C^2 + K_{\mathrm{a}}^2)(P^2 + K_{\mathrm{IP}}^2)}(S - C)$$
$$\frac{\mathrm{d}R}{\mathrm{d}t} = k_R \left(\frac{K_{\mathrm{i}}^2}{K_{\mathrm{i}}^2 + C^2} - R \right)$$

Ca^{2+} flux leaking from ER (1):

$$J_{\mathrm{leak}} = k_{\mathrm{leak}}(S - C)$$

Ca^{2+} flux through the SERCA pump (1):

$$J_{\mathrm{SERCA}} = k_{\mathrm{SERCA}} C$$

Ca^{2+} flux through PMCA pump (1):

$$J_{\mathrm{PMCA}} = k_{\mathrm{PMCA}} C$$

Ca^{2+} entry fluxes from the extracellular space (1):

$$J_{\mathrm{in}} = v_{\mathrm{in}} + v_r \frac{P^2}{K_r^2 + P^2}$$

Current through voltage-gated Ca^{2+} channels (2):

$$I_{\mathrm{Ca}} = g_{\mathrm{Ca}} m^2 h (V - E_{\mathrm{Ca}})$$
$$\frac{\mathrm{d}m}{\mathrm{d}t} = \frac{m_\infty - m}{\tau_m}$$
$$\frac{\mathrm{d}h}{\mathrm{d}t} = \frac{h_\infty - h}{\tau_h}$$
$$m_\infty = \frac{1}{1 + \exp(-\frac{V+25}{10})}$$
$$\tau_m = \frac{0.001}{\exp\left(-\frac{V+23}{20}\right) + \exp\left(\frac{V+23}{20}\right)} + 0.00005$$
$$h_\infty = \frac{1}{1 + \exp(\frac{V+28}{5})}$$
$$\tau_h = \frac{0.03}{\exp\left(-\frac{V}{20}\right) + \exp\left(\frac{V}{20}\right)} + 0.021$$

Current through voltage-gated K^+ channels (2):

$$I_{\mathrm{K}} = g_{\mathrm{K}} n^4 (V - E_{\mathrm{K}})$$
$$\frac{\mathrm{d}n}{\mathrm{d}t} = \frac{n_\infty - n}{\tau_n}$$
$$n_\infty = \frac{1}{1 + \exp(-\frac{V+18.5}{23})}$$
$$\tau_n = \frac{0.0015}{\exp\left(-\frac{V+10}{25}\right) + \exp\left(\frac{V+10}{25}\right)} + 0.015$$

Leak current:

$$I_{\mathrm{L}} = g_{\mathrm{L}}(V - E_{\mathrm{L}})$$

Parameters. The related parameters are shown in Table S1. Sensitivity analysis on parameters involved in the slow pathway (Fig. S1) shows that our model is insensitive to the change of these parameters in a large range (0.8× - 1.2×). Parameter sweeping on the two major factors of the fast pathway, g_{Ca} and g_{K} (Fig. S2), shows that they are affecting the equilibrium of the action potential (AP), and in a large range of the combination of values of g_{Ca} and g_{K}, a post-stimulation AP can be triggered, of which the lag time is smoothly changing with the parameter values.

Calcium fluxes and ion currents. Fig. S3 includes the supplementary plots of Fig. 3B and 3C of the main text, showing the calcium fluxes and ion currents related to the dynamics.

Equilibrium requirements. To maintain the cell in the equilibrium state with no external stimulation, several equilibrium conditions need to be held at the initiation.

The equilibrium of membrane currents:

$$I_{\mathrm{Ca}} + I_{\mathrm{K}} + I_{\mathrm{L}} = 0$$

The equilibrium of Ca^{2+} fluxes through the cell membrane:

$$J_{\mathrm{in}} - J_{\mathrm{PMCA}} - \alpha I_{\mathrm{Ca}} = 0$$

The equilibrium of Ca^{2+} fluxes through the ER membrane:

$$J_{\mathrm{IPR}} + J_{\mathrm{leak}} - J_{\mathrm{SERCA}} = 0$$

Initial values of the dynamical variables are set as equilibrium values of these equations.

Multicellular model details

Calibration of the size of muscle sheets. To simulate calcium signaling in the whole-body muscle sheets, we construct ectodermal and endodermal networks of *Hydra* epitheliomuscular cells. The number of muscle cells of *Hydra* varies considerably with body size (3). For a representative *Hydra* of length of 1.38 mm, we counted 62 cells longitudinally and 30 (15×2) - 34 (17×2) cells circumferentially, depending on the longitudinal location (Fig. S4). We approximate the body column as a cylinder composed of 30×60 square cells, of which the side length is 30 μm; the lateral sheet edges are connected and the topmost and bottommost cell rows are taken to be isolated from the environment. Cells within a layer are connected to their neighbours via gap junctions.

Effects of stimulation strength on wave propagation. As shown in Table S1, we set the stimulation strength of the slow pathway ($v_{\mathrm{PLC}\beta}$) as 1.0 μM/s and that of the fast pathway (I_{stim}) as 0.02 mA/cm^2. To explore how these values affect the results, we sweep them over an order of magnitude (0.1 - 1.0 for the slow wave; 0.004 - 0.04 for the fast wave) and plot how these inputs influence the longitudinal [Ca^{2+}] propagation, given stimulation of a local (2×2 cells) domain at the center of a 30×60 muscle sheet (Fig. S5). The wavefront index is defined as the maximum index of cells whose [Ca^{2+}] concentration is higher than a threshold (0.055 μM). The results show a clear phase transition of fast wave propagation when I_{stim} is between 0.016 - 0.02 mA/cm^2, which does not appear in the slow wave.

When the stimulation strengths are small, both the slow pathway and fast pathway propagate in a form of diffusion (not shown); when the strengths are large, the slow pathway gradually exhibits a diffusive-wave propagation pattern, while the fast pathway suddenly transitions to a regenerative-wave propagation pattern when the input strength exceeds a threshold.

Effects of gap-junctional coupling coefficients on wave propagation. We explore the effects of the gap-junctional coupling coefficients $g_{\mathrm{IP_3}}$ and g_{c} (in units of s^{-1}) by tuning their values along with longitudinal and circular directions and visualizing how they will affect the propagation range of the slow waves and the propagation speed of the fast waves, with the values of all other parameters fixed. Both are again initiated by stimulating a domain of 2×2 cells at the center of a 30×60 muscle sheet (Fig. S6). In both cases, a larger coupling coefficient facilitates the propagation in that direction, and reduces the propagation in the orthogonal direction. The default values used in our simulation are: $g_{\mathrm{c}} = 1000$ s^{-1} for both longitudinal and circular directions; $g_{\mathrm{IP_3}} = 2$ s^{-1} for the longitudinal direction and 0.1 s^{-1} for the circular direction.

The reason that use different criteria to measure the slow and fast waves is due to the different natures between them: the amplitude of slow wave is significantly decaying with the propagation distance and ceases at some point, and we found the average speed (which is strongly affected by how we set the threshold to define wavefront) is not a good metric to measure the strength of wave propagation, instead, the farthest wavefront which shows "how far" the wave can propagate can perfectly reflect that; as for the fast wave, since it's global which means it finally activates all cells, the farthest wavefront is just the border of the sheet which is trivial, so the speed which shows "how fast" the wave can reach the border plays a good metric.

Effects of intracellular parameters on wave propagation. Besides the coupling coefficients, some intracellular parameters that influence the strength or duration of the calcium dynamics can also affect wave propagation. We select some significant parameters here and explore their effects by sweeping them and measure the effects on propagation range (slow wave) or speed (fast wave) along the longitudinal direction under local stimulation (2×2 cells at the center) (Fig. S7), with all other parameters fixed. Fig. S7A shows that both larger k_{IPR} or smaller k_{deg} can make the wave propagate farther – this is expected as a larger k_{IPR} indicates a larger calcium release from ER stores when IPR is activated by IP_3, and a smaller k_{deg} means the IP_3 decays more slowly. Both effects will cause stronger calcium dynamics and facilitate wave propagation. Fig. S7B shows that increasing either k_{SERCA} or k_{PMCA} limits the maximum wave range, which is again reasonable since both factors are proportional to the extent that Ca^{2+} is recycled (k_{SERCA}) or extruded (k_{PMCA}) from the cytosol; therefore their increase results in a reduction in cytosolic Ca^{2+} concentration and hinders wave propagation. Fig. S7C shows larger g_{Ca} greatly facilitates the propagation speed of the fast wave, which can be due to the increase of Ca^{2+} influx from the extracellular space; larger g_{K} can increase the Ca^{2+} efflux from the cytosol to extracellular space, thus reducing the strength of the calcium dynamics and hindering fast wave propagation.

Force generation model details

As given in Eq. 2 in the main text, we use the Hai-Murphy model to transform the Ca^{2+} dynamics into contracting stress patterns, and set different parameters for the ectoderm (phasic muscle) and endoderm (tonic muscle). The details of these parameters are shown in Table S2. Parameters are tuned to fit the length change of the model to that of the corresponding measured *Hydra*, based on the ranges and values provided in (4) and (5).

Biomechanics details

The parameters of our biomechanical model, constructed in COMSOL Multiphysics® 5.3a, are shown in Table S3. The configurations of the solver are shown in Table S4. An additional example simulation result with a different neural drive is shown in Fig. S8.

Effects of parameter variations on length change

Fig. S9 shows how some key parameters can affect the length change of the model under a series of contraction pulse stimuli, with other parameters fixed. The stimulation train is extracted from measurements of real *Hydra*. These parameters are selected since they reflect pivotal physical properties that align with the focus of our model, and our simulation results match their definitions and the expectation: endodermal c_{half} represents the half-saturation $[Ca^{2+}]_i$ for MLCK activation in endoderm, of which a larger value means a lower sensitivity of the response of endodermal stress to the calcium concentration, thus a smaller resistance of the body to the contraction (Fig. S9A); endodermal k_7 represents the detachment rate of the latch-bridge state of endodermal myoneme, of which a larger value means a longer maintenance of contraction in endoderm, thus a longer time for the body to recover after contracted (Fig. S9B); endodermal K_F represents the stress strength that generated by per unit of latch bridge state ratio in the endoderm, of which a larger value means a stronger endodermal stress, thus a larger resistance of the body to the contraction, and such a relationship is linear, different from that of c_{half} (Fig. S9C); relaxation time represents the viscosity of the muscle material, of which a larger value means a stronger and slower resistance to and recovery from the stress caused deformation of the body (Fig. S9D). We preferably select the parameters of the endoderm for sensitivity analysis because the tonic property provides more variant and complex effects on the behaviors compare to the phasic ectoderm.

Model reduction

To explore the high-level properties of the biophysical model, we apply a pointwise (a domain of 2×2 cells) pulse stimulation at the middle of the muscle sheet and plot the generated wave dynamics ($[Ca^{2+}]_i$) along with the center longitudinal line for both slow and fast dynamics (Fig. S10A, B). Based on the plots, we propose a Green's function form for both slow and fast waves:

$$G(\rho,t) = A\Theta\left(t-\frac{\rho}{v}\right)\left(1-e^{-\frac{t-\rho/v}{\tau_{\mathrm{inc}}}}\right)e^{-\frac{t-\rho/v}{\tau_{\mathrm{dec}}}}e^{-\frac{\rho}{\rho_c}}$$

where $\Theta(\cdot)$ is the Heaviside function, ρ is the distance between a point and the source, t is the time since the stimulation, A is the maximum amplitude constant, v is the velocity of the wave propagation, τ_{inc} is the time constant of the increasing phase, τ_{dec} is the time constant of the decreasing phase, ρ_c is the scaling constant of the amplitude. To represent the anisotropy of the coupling coefficients of slow waves, we define the distance as $\rho = \sqrt{(c_w x)^2 + y^2}$, where x, y are the distance between the point and the source respectively in the circular and longitudinal direction, c_w is a warping coefficient that represents the anisotropy. Warping the space is equivalent to defining directional velocities but simpler to represent.

We fit the Green's function by sweeping over the key parameters ($A, v, \tau_{\mathrm{inc}}, \tau_{\mathrm{dec}}, \rho_c$ and c_w) to match some selected targets: we firstly select a point on the sheet, then sweep τ_{inc}, τ_{dec} and A to fit its amplitude and the time of its increasing and decreasing phases, by picking the combination that minimizes the difference between the Green's function and the biophysical model. Then we select two points that are far from each other, then sweep v, ρ_c and c_w to fit their time difference and amplitude difference, picking the pair that gives a closest result with the biophysical model. The optimized values of these parameters are

shown in Table S5, and the spatiotemporal pattern of the Green's function along with the center longitudinal line for the slow and fast dynamics are shown in (Fig. S10C, D).

Though the Green's function reproduces some characteristics of the biophysical model, its biggest limitation is it can only represent linear responses. However, our biophysical model includes strong nonlinearity in both single-cellular dynamics and the inter-cellular interactions. For instance, the refractory period of the action potential and the depletion of ER store make that when two fast waves or two slow waves collide with each other, they exhibit some extent of canceling (an example of the fast wave is shown in Fig. S11). Also, the wave-shapes of different cells differ a lot in the biophysical model simulation, so some parameters that are fitted with one or two arbitrary points are not generally accurate. Better simplification needs incorporating more nonlinearity and therefore greatly increases the problem complexity, and our attempt with Green's functions is a start that may inspire the future work.

Supplementary results

Animation of the whole simulation pipeline. A movie showing the simulation results from neural activity to behaviors (Movie S1), as a supplement of Fig. 7 in the main text.

Simulated movement without assuming phasic and tonic muscle types. A movie showing the simulated "contraction" of our model when we directly apply the transformed stress from calcium dynamics on the biomechanical model, without distinguishing the ectoderm and the endoderm with phasic/tonic muscle types (Movie S2).

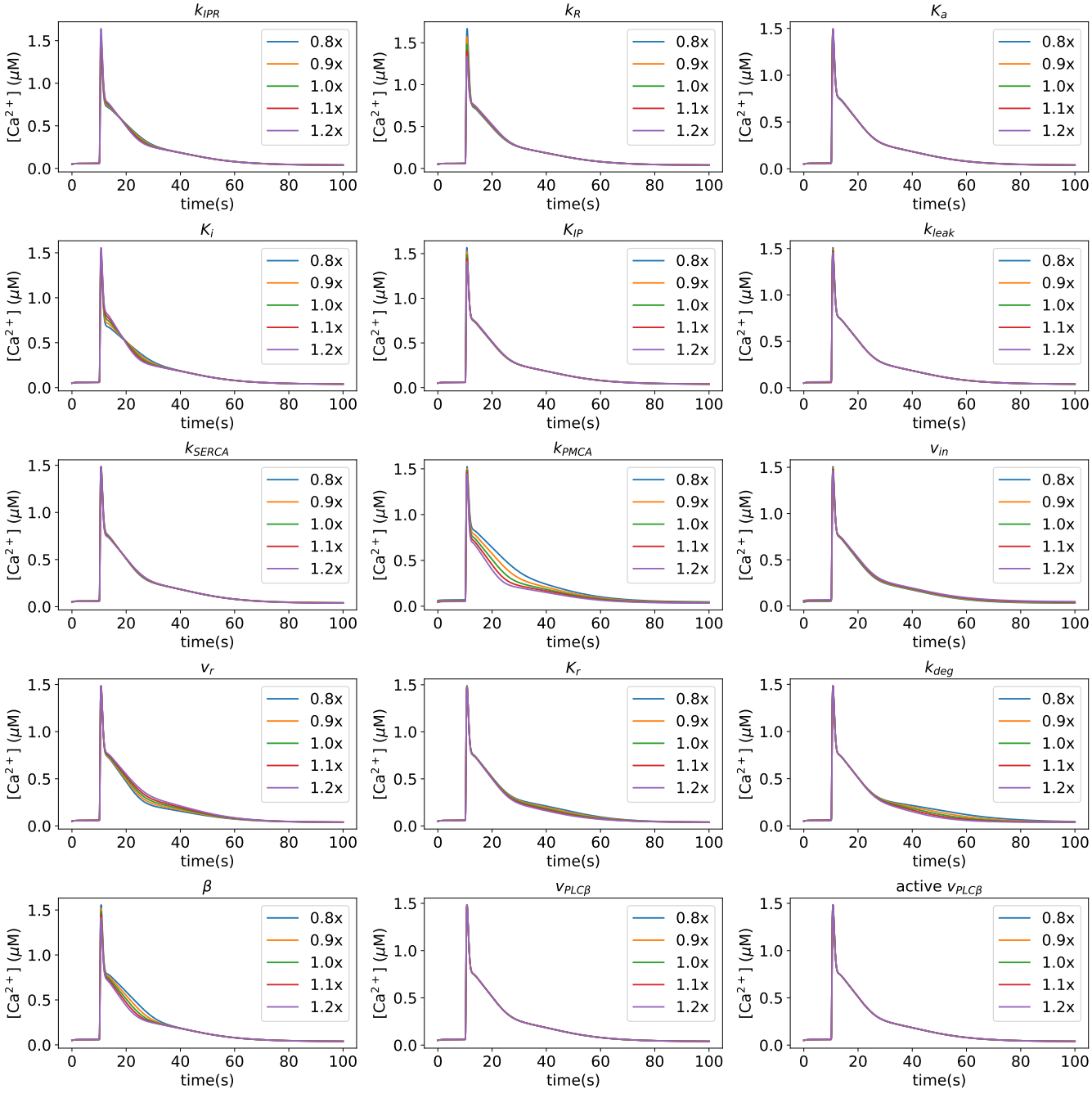

Fig. S1. Effects on [Ca^{2+}] by tuning parameters that are involved in a slow pathway. Each parameter is swept from 0.8× to 1.2× of the default value, with a step size as 0.1×. This shows the subtle variation in dynamics due to these parameter choices.

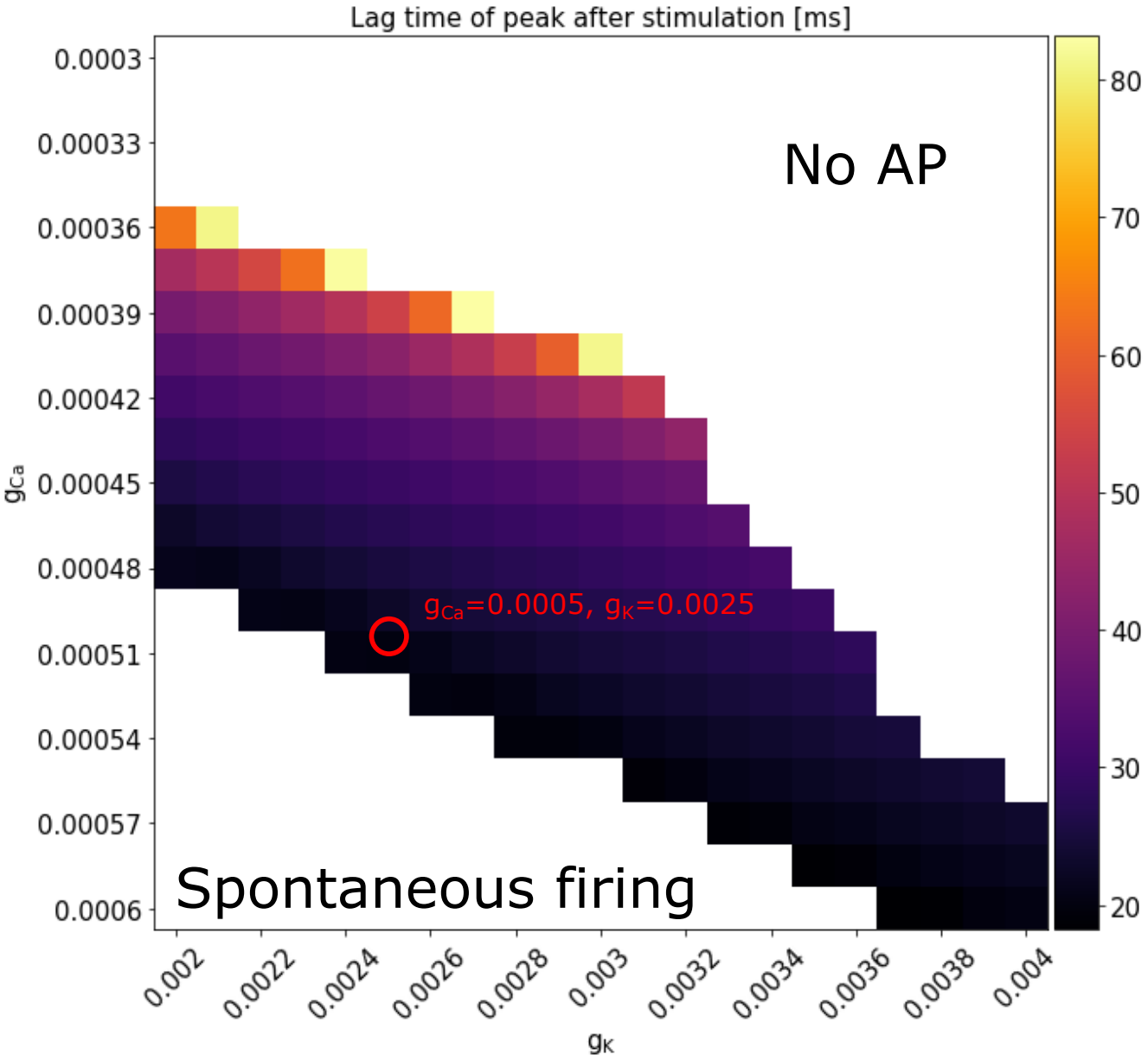

Fig. S2. Effects of different values of channel conductances g_{Ca} and g_K on the lag time of the action potential peak after the stimulation. The choice used in the final model is circled out, showing that there is a range of conductances that give rise to reasonable lag times.

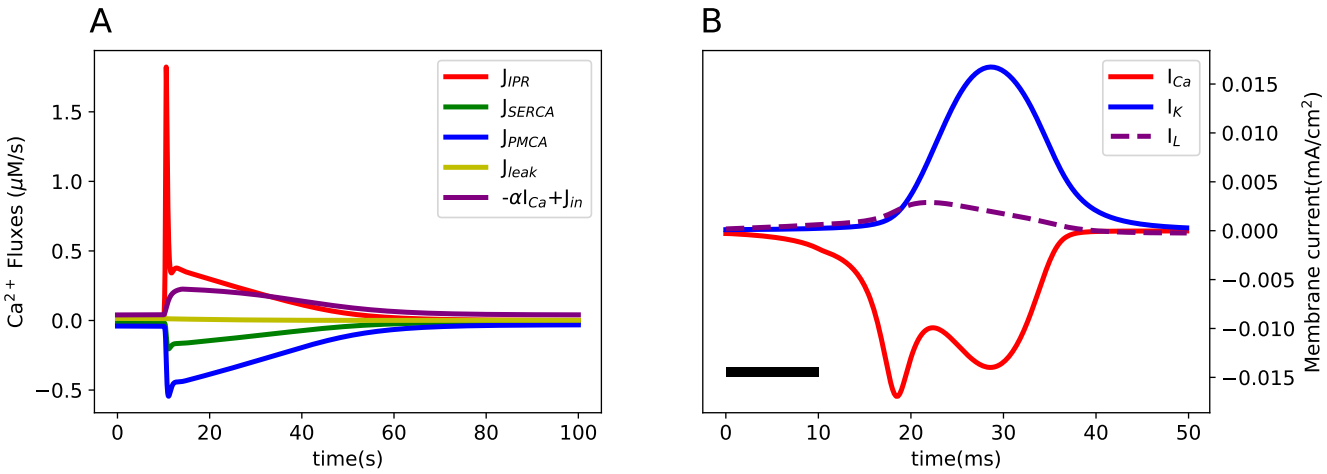

Fig. S3. Calcium fluxes (*A*) and ion currents (*B*), respectively correspond to Fig. 3A and Fig. 3B in the main text.

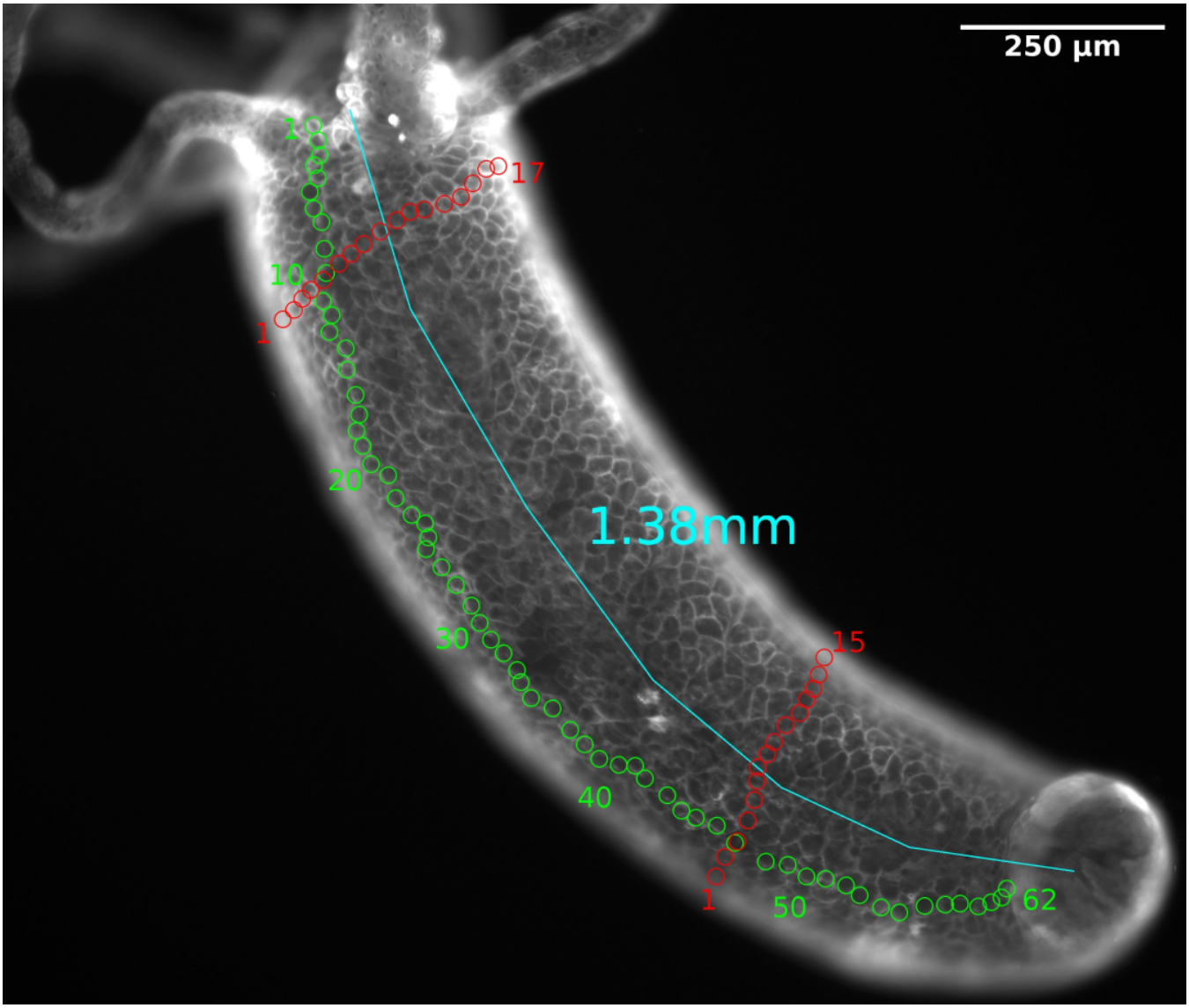

Fig. S4. Cell counting and length measurement in a small *Hydra*. Green circles are the counts in longitudinal direction and red colors are the counts in circumferential direction.

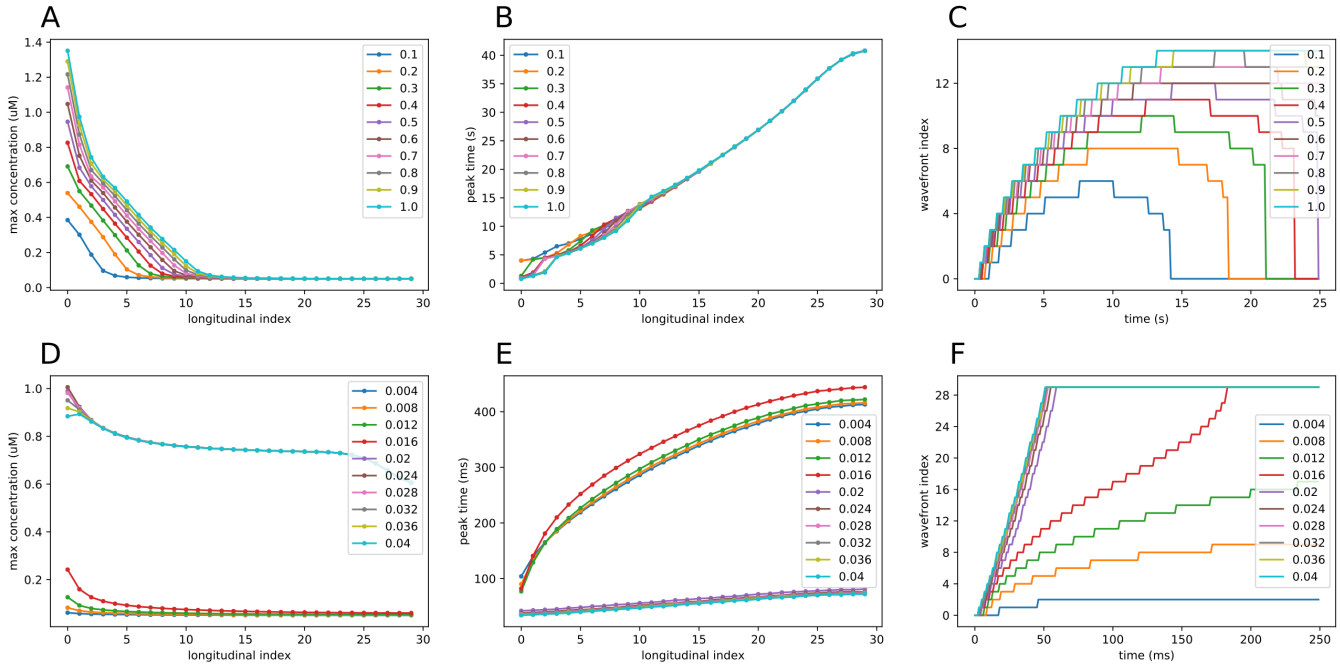

Fig. S5. Observables of [Ca^{2+}] propagation change with different stimulation strengths of the slow wave (*A* - *C*) and the fast wave (*D* - *F*), including the distribution of maximum concentration (amplitude) over longitudinal index (*A*, *D*), the arrival time of peaks versus the longitudinal index (*B*, *E*) and the wavefront index change over time (*C*, *F*).

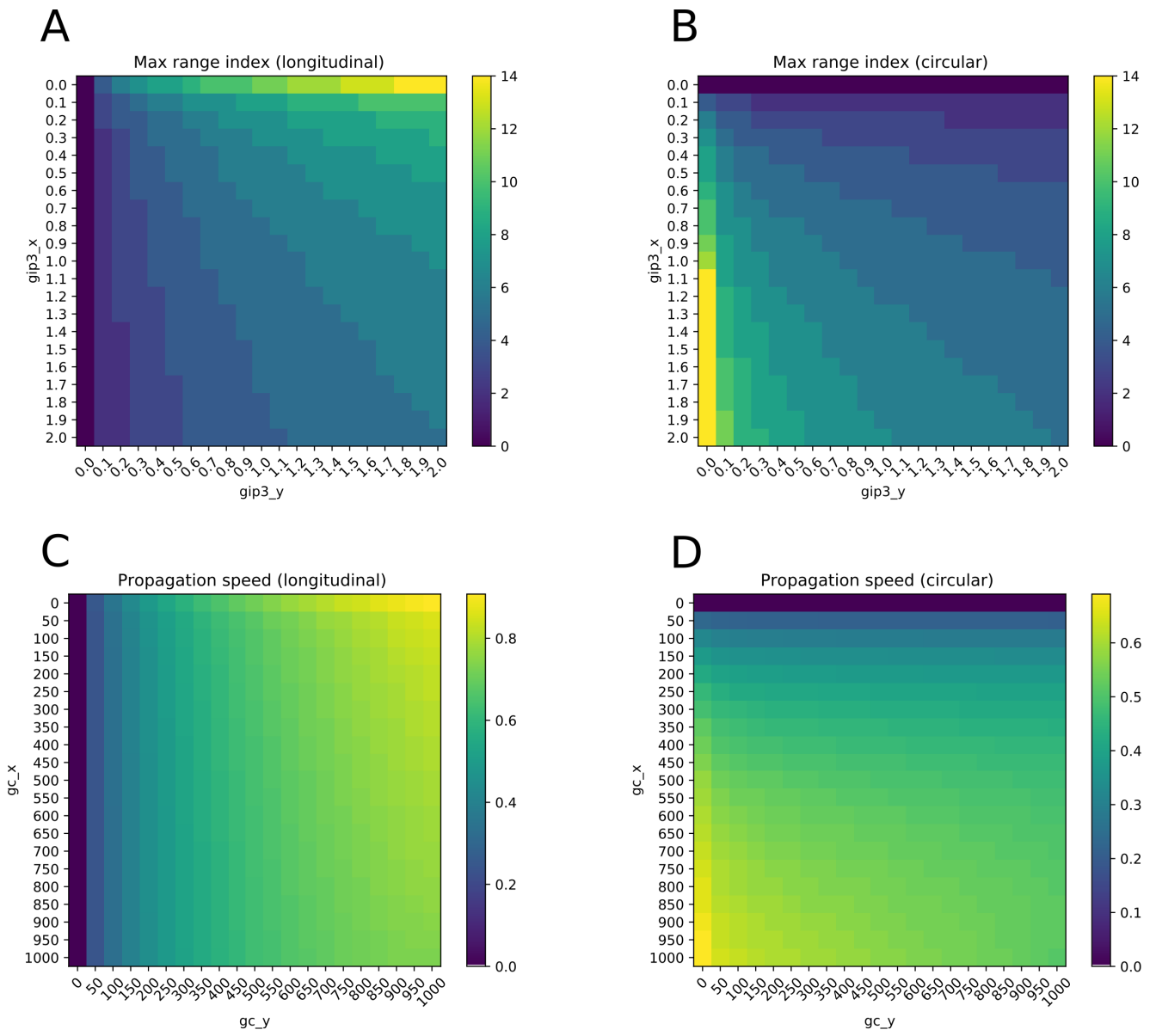

Fig. S6. Effects of gap-junctional coupling coefficients on wave propagation. (*A*) The effect of g_{IP_3} on the longitudinal range of the slow wave. (*B*) The effect of g_{IP_3} on the circular range of the slow wave. (*C*) The effect of g_{c} on the longitudinal propagation speed of the fast wave. (*D*) The effect of g_{c} on the circular propagation speed of the fast wave.

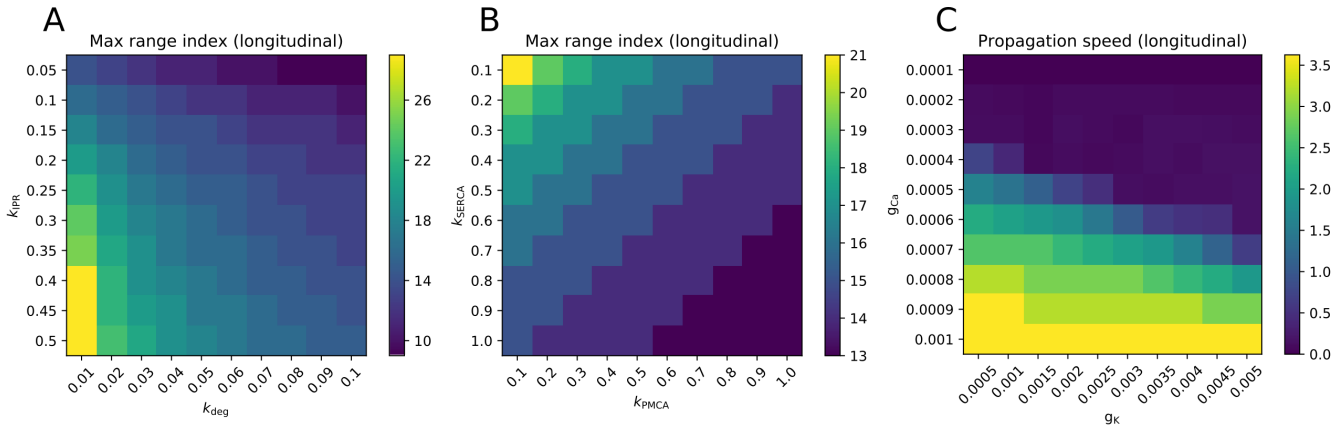

Fig. S7. Effects of intracellular parameters on wave propagation. (*A*) Effects of sweeping k_{IPR} and k_{deg} on the longitudinal range of the slow wave. (*B*) Effects of sweeping k_{SERCA} and k_{PMCA} on the longitudinal range of the slow wave. (*C*) Effects of sweeping g_{Ca} and g_{K} on the longitudinal propagation speed of the fast wave.

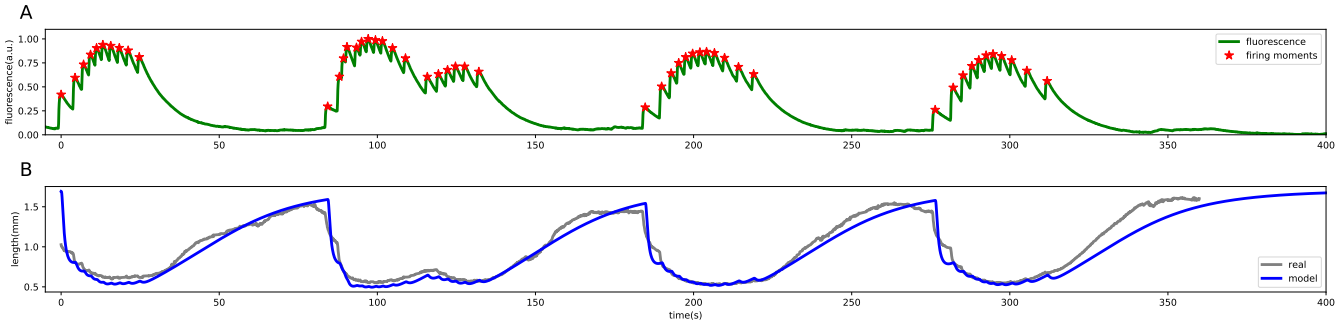

Fig. S8. Simulation following another video where two bursts are consecutive. (A) whole-frame fluorescence trace and neural firing moments; (B) comparison between length evolution of the model and the real *Hydra* in the video.

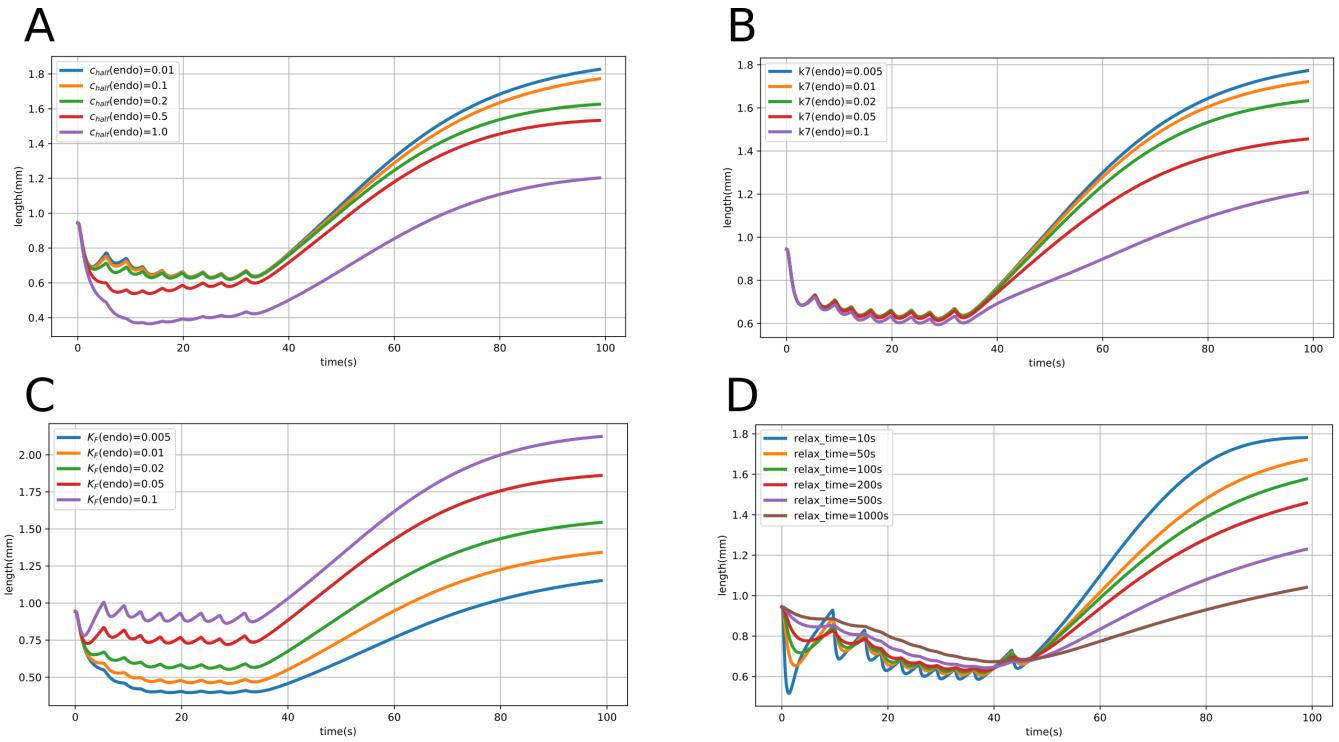

Fig. S9. Effect on the length change by sweeping different parameters: (*A*) Endodermal c_{half}; (*B*) Endodermal k_7; (*C*) Endodermal K_F; (*D*) relaxation time (representing viscosity).

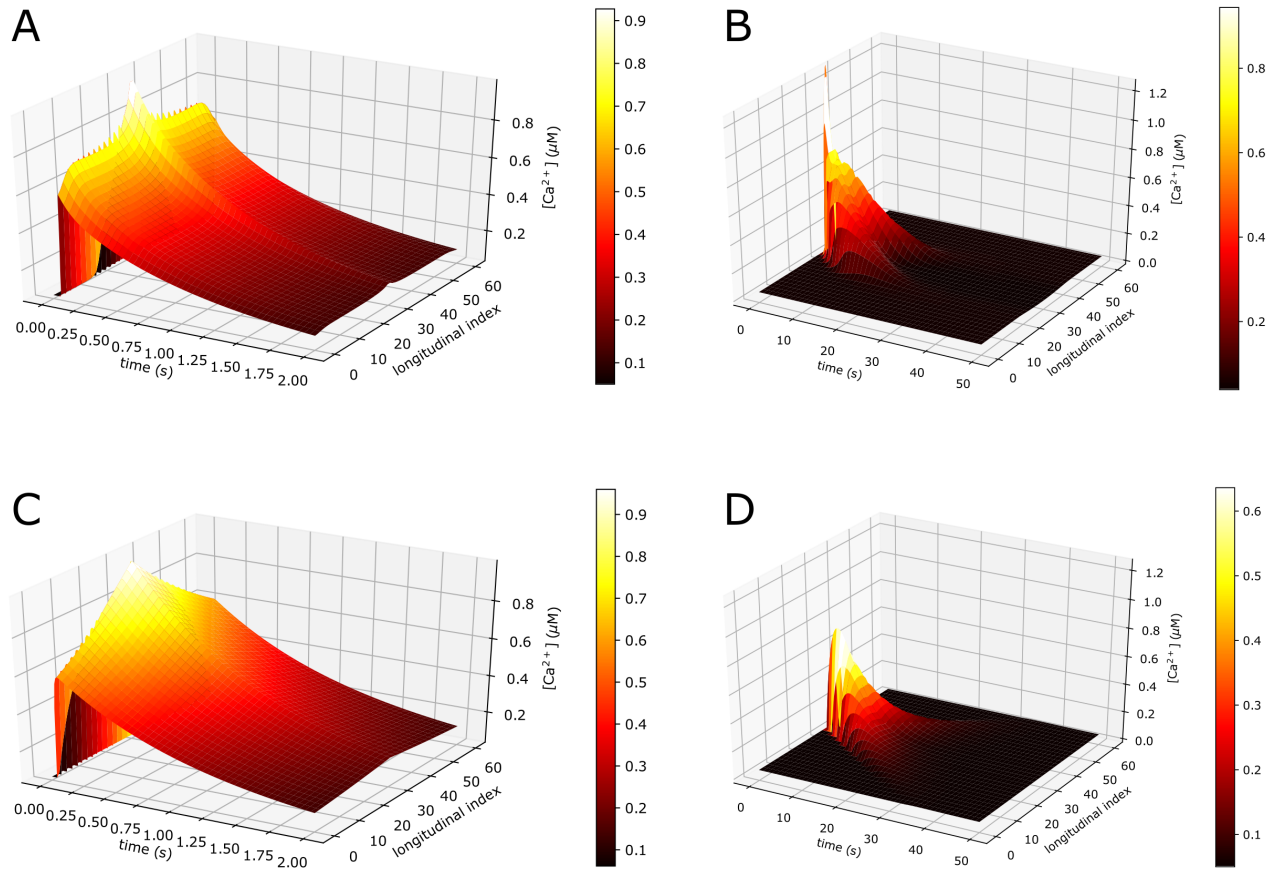

Fig. S10. Spatiotemporal pattern of the impulse response of the longitudinal center-line points in the biophysical model and Green's function. (*A*) Biophysical model response to a fast pathway stimulation. (*B*) Biophysical model response to a slow pathway stimulation. (*C*) Green's function of the fast wave. (*D*) Green's function of the slow wave.

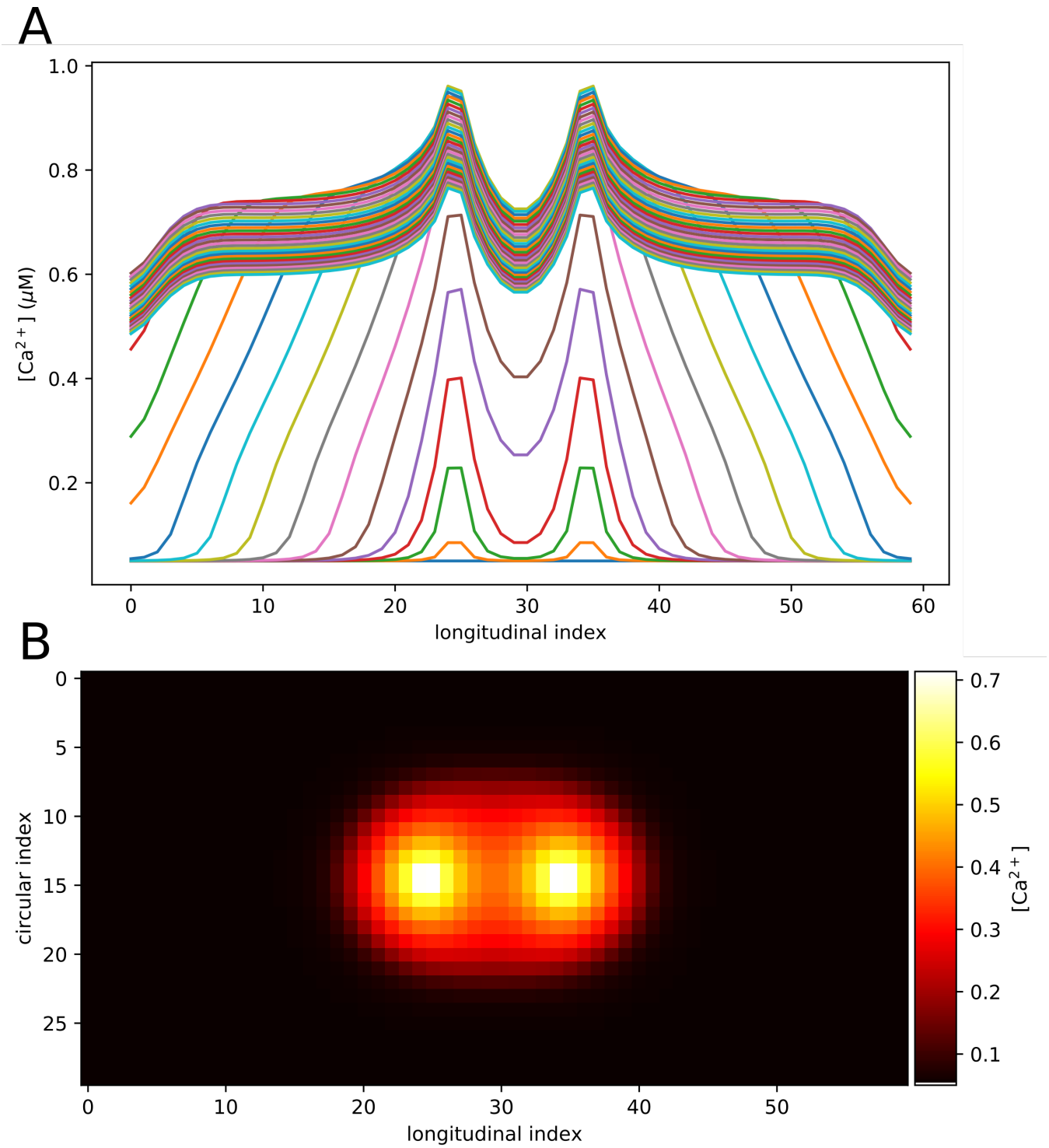

Fig. S11. Nonlinearity exhibited by the interaction of two pointwise-stimulated fast waves. (*A*) Traces showing how $[Ca^{2+}]_i$ evolves, in which each curve represents a time point. (*B*) Snapshot of the muscle sheet at 25 ms after the stimulation, in which two waves cancel each other at the middle.

Table S1. Parameters used in the single cell model

Parameter	Description	Value	Unit	Source
k_{IPR}	Rate constant of Ca^{2+} release through IPR	0.2	s^{-1}	(1)*
k_R	Rate constant of IPR inactivation	4	s^{-1}	(1)
K_{a}	Half-saturation constant for Ca^{2+} activation of IPR	0.2	μM	(1)
K_{i}	Half-saturation constant for Ca^{2+} inhibition of IPR	0.2	μM	(1)
K_{IP}	Half-saturation constant for IP_3 activation of IPR	0.3	μM	(1)
k_{leak}	Rate constant of Ca^{2+} leak from ER	0.0002	s^{-1}	(1)*
k_{SERCA}	Rate constant of SERCA pump	0.3	s^{-1}	(1)*
k_{PMCA}	Rate constant of PMCA pump	0.8	s^{-1}	(1)*
v_{in}	Rate of Ca^{2+} leak across the plasma membrane	0.04	μM/s	(1)*
v_{r}	Maximal rate of activation-dependent Ca^{2+} influx	0.2	μM/s	(1)
K_{r}	Half-saturation constant for activation-dependent Ca^{2+} entry	1	μM	(1)
$v_{\mathrm{PLC}\beta}$	Rate of PLCβ	0.002 - 1.0	μM/s	(1)*
k_{deg}	Rate constant of IP_3 degradation	0.05	s^{-1}	(1)*
α	Current conversion factor	5182.13	μM·cm^2/mC	(6)
β	Ratio of the volumes of cytoplasm and ER	20	1	(1)
g_{Ca}	Maximal conductance of I_{Ca}	0.0005	S/cm^2	(6)*
E_{Ca}	Reversal potential of I_{Ca}	51	mV	(6)
g_{K}	Maximal conductance of I_{K}	0.0025	S/cm^2	(6)*
E_{K}	Reversal potential of I_{K}	-75	mV	(6)
g_{L}	Conductance of I_{L}	0.000036	S/cm^2	*
E_{L}	Reversal potential of I_{L}	-55	mV	*
C_m	Membrane capacitance per unit area	1	μF/cm^2	(6)
I_{stim}	Current through ligand-gated ion channels	0 - 0.02	mA/cm^2	(6)

* Modified or tuned in the physiological plausible range to match the time scales of single cellular dynamics and wave propagation. Detailed sensitivity analysis is discussed and shown in Fig. S1 and Fig. S2.

Table S2. Parameters used in the modified Hai-Murphy model

Parameter	Description	Value	Unit
k_1	Rate of $M \rightarrow Mp$	$\frac{C^{n_M}}{c_{\text{half}}^{n_M} + C^{n_M}}$	s^{-1}
k_2	Rate of $Mp \rightarrow M$	0.15	s^{-1}
k_3	Rate of $A + Mp \rightarrow AMp$	16 (ecto) / 0.4 (endo)	s^{-1}
k_4	Rate of $AMp \rightarrow A + Mp$	4 (ecto) / 0.05 (endo)	s^{-1}
k_5	Rate of $AMp \rightarrow AM$	k_2	s^{-1}
k_6	Rate of $AM \rightarrow AMp$	k_1	s^{-1}
k_7	Rate of $AM \rightarrow A + M$	0.75 (ecto) / 0.015 (endo)	s^{-1}
c_{half}	Half-saturation $[\text{Ca}^{2+}]_i$ for MLCK activation	0.85 (ecto) / 0.15 (endo)	μM
n^M	Hill coefficient of Ca^{2+} activation of MLCK	4	1
K_F	Proportional coefficient of active stress generation	3.3 (ecto) / 0.3 (endo)	N/mm^2

Table S3. Parameters used in the COMSOL model

Parameter	Value	Unit
Top half sphere radius	97.5	μm
Bottom half sphere radius	97.5	μm
Body cylinder height	650	μm
Thickness	19.5	μm
Density of Enclosed Fluid	1000	kg/m^3
Density of Muscle	1200	kg/m^3
Lamé parameter μ of Muscle	3.336	kPa
Lamé parameter λ of Muscle	1.664	GPa
Initial bulk modulus of muscle	1.667	GPa
Relaxation time of muscle	70	s
Temperature	293.15	K
Time step	0.1	s

Table S4. COMSOL solver configurations

Option	Value
Time stepping method	BDF
Steps taken by solver	Intermediate
Initial step	0.001 s
Maximum step	0.1 s
Maximum BDF order	2
Minimum BDF order	1
Event tolerance	0.01
Nonlinear controller	True
Singular mass matrix	Maybe
Consistent initialization	Backward Euler
Fraction of initial step fore Backward Euler	0.001
Error estimation	Exclude algebraic
Absolute tolerance global method	Scaled
Tolerance method	Factor
Tolerance factor	0.05
Update scaled absolute tolerance	True
Solver	MUMPS
Memory allocation factor	1.2
Preordering algorithm	Automatic
Row preordering	True
Reuse preordering	True
Use pivoting	On
Pivot threshold	0.1
Out-of-core	Automatic
Memory fraction for out-of-core	0.99
In-core memory method	Automatic
Minimum in-core memory	512 MB
Used fraction of total memory	0.8
Internal memory usage factor	3
Check error estimate	Automatic
Factor in error estimate	400
Iterative refinement	True
Maximum number of refinements	15
Matrix symmetry	Automatic
Matrix format	Automatic
Row equilibration	True
Null-space function	Automatic
Orthonormal block limit	10000000
Store last residual	Off
Solver log	Normal
Log sampling (wall-clock)	0.005 s
Assembly block size	1000
Stop when undefined mathematical operation is detected	True
Nonlinear method	Constant (Newton)
Damping factor	1
Limit on nonlinear convergence rate	0.9
Jacobian update	On every iteration
Termination technique	Iterations or tolerance
Number of iterations	1
Tolerance factor	0.1

Table S5. Parameters of Green's function after fitting

Parameter	Value (fast)	Value (slow)	Unit
A	0.9843	5.7737	μM
v	731	0.9	cell/s
τ_{inc}	0.008	9.3	s
τ_{dec}	1.01	3.9	s
ρ_c	55	5.2	μM
c_w	1	4.9	1

Movie S1. Simulation results from neural activity to muscle dynamics to behaviors.

Movie S2. Simulation results from directly applying the transformed stress on the biomechanical model without distinguishing phasic/tonic muscle types.

References

1. T Höfer, L Venance, C Giaume, Control and plasticity of intercellular calcium waves in astrocytes: a modeling approach. *J. Neurosci.* **22**, 4850–4859 (2002).
2. PM Diderichsen, SO Göpel, Modelling the electrical activity of pancreatic α-cells based on experimental data from intact mouse islets. *J. biological physics* **32**, 209–229 (2006).
3. CN Tzouanas, S Kim, KN Badhiwala, BW Avants, JT Robinson, Hydra vulgaris shows stable responses to thermal stimulation despite large changes in the number of neurons. *Iscience* **24**, 102490 (2021).
4. S Han, et al., Evidence for absence of latch-bridge formation in muscular saphenous arteries. *Am. J. Physiol. Circ. Physiol.* **291**, H138–H146 (2006).
5. M Yochum, J Laforêt, C Marque, An electro-mechanical multiscale model of uterine pregnancy contraction. *Comput. biology medicine* **77**, 182–194 (2016).
6. C Mahapatra, KL Brain, R Manchanda, A biophysically constrained computational model of the action potential of mouse urinary bladder smooth muscle. *PloS one* **13** (2018).